Journal of the Civil Engineering Forum, May 2026, 12(2):152-169
DOI 10.22146/jcef.22499
Available Online at https://jurnal.ugm.ac.id/v3/jcef/issue/archive

A Flexural Behavior of Full-Scale RC Beam Strengthened Using Glass Fiber Reinforced Polymer: Experimental Research

Oktalia Wuranti Putri[1], Angga Fajar Setiawan[1*], Suprapto Siswosukarto[1], Muhammad Akhsin Muflikhun[2], Noorsuhada Md Nor[3], Muslikh[4]
[1]Department of Civil and Environmental Engineering, Universitas Gadjah Mada, Yogyakarta, INDONESIA
[2]Department of Mechanical and Industrial Engineering, Universitas Gadjah Mada, Yogyakarta, INDONESIA
[3]Faculty of Civil Engineering, Universiti Teknologi MARA, Cawangan Pulau Pinang, Kampus Permatang Pauh, Pulau Pinang, MALAYSIA
[4]Department of Civil Engineering, Universitas Cokroaminoto, Yogyakarta, INDONESIA
*Corresponding author: angga.fajar.s@mail.ugm.ac.id

SUBMITTED 20 June 2025 **REVISED** 13 October 2025 **ACCEPTED** 27 October 2025

ABSTRACT Reinforced Concrete (RC) structures, though strong and economical, may need to be strengthened due to increased load demand for upgraded room functions. Strengthening an RC beam element with Glass Fiber Reinforced Polymer (GFRP) offers flexural strength enhancement, corrosion resistance, and cost efficiency. However, the study that considers the full-scale dimension of a beam strengthened with GFRP is still limited. Therefore, more studies on the flexural strength enhancement of RC beams with GFRP need to be conducted. This research investigated the flexural performance of full-scale RC beams strengthened with externally bonded GFRP. This study involved testing five beam specimens, each with a different number of GFRP layers attached to the outermost tensile zone of the cross-section. Flexural testing was conducted using a four-point bending setup with a loading–unloading scheme to capture the specimens' elastoplastic behavior, considering recovery during unloading. The analyzed parameters included stiffness, yield strength, debonding strength, ultimate strength, and ductility. Furthermore, the flexural strength was predicted through analytical calculations based on the fiber section method, while the shear strength was estimated following the ACI 318M-14 code. The experimental results showed that GFRP strengthening considerably increased stiffness and first flexural strength of RC beams as a proportion of the number of layers during the pre-debonding state. Despite the debonding occurrence initiating a temporary lapse in the role of GFRP at 0.67% to 0.93% of displacement-span-ratio, it decreased the flexural resistance momentarily. Then, the strengthened beams with two-to-four-layer GFRP still exhibited second ultimate flexural strength enhancement within the range 14.35% to 39.22%. Furthermore, GFRP strengthening generally preserved beam ductility at the second ultimate flexural strength due to the catenary action from debonded GFRP in the plastic hinge zone. Thus, additional GFRP for strengthening RC beams could be effective in the case of a positive bending moment to enhance the stiffness, strength, and ductility.

KEYWORDS Reinforced concrete beam; Glass fiber reinforced polymer; Flexural strengthening; Ductility; Full-scale; Debonding.

1 INTRODUCTION

Reinforced concrete structures are used in various building constructions because the components have good compressive and tensile strength. The construction of this structure also requires lower costs than other structures (Mosley et al., 2012). When used, the problem in reinforced concrete structures comes from a decrease in strength due to changes in loading, building functions, deterioration of materials, or recording of increasing earthquake intensity (Tanjung and Putri, 2023). Moreover, corrosion of steel reinforcement can reduce the bond strength between concrete and steel, compromising the structure's dynamic and static performance (Rahman et al., 2024). Therefore, structural strength improvement of reinforced concrete structures needs to be conducted to extend the service life and ensure sufficient load resistance.

A type of load resistance of reinforced concrete beams is flexural strength, which is achieved through sufficient strength and structural stability. If the flexural strength of the existing beam is insufficient to resist the load demand, additional flexural strengthening should be considered. Some methods for additional reinforced concrete beams include external steel attachment, adding external prestressing steel, combining longitudinal reinforcement to the concrete tensile surface, and applying Fiber Reinforced Polymer (FRP) to the concrete surface (Ali et al., 2021). FRP is a composite material made of continuous fibers implanted in a polymer matrix, allowing it to compensate for the brittle nature of concrete and improve ductility (Mohd Hashim et al., 2013). In addition, FRP is lightweight, noncorrosive, and possesses high tensile strength (American Concrete Institute, 2017). A type of

FRP is Glass Fiber Reinforced Polymer (GFRP), a composite material consisting of polymer matrix sheets made from resins and glass fibers (ACI Committee 440, 2006). GFRP is alkaline and nonreactive to chlorides, has a high weight-to-strength ratio, is nonconductive to temperature, and is relatively cheaper than other types of FRP (Saravanakumar et al., 2014).

Previous research on flexural strengthening of reinforced concrete beams with GFRP was conducted by Nayak et al. (2018). In the analysis, the beams with dimensions 120 mm $\times$ 150 mm of cross-section and 1000 mm span length with the U-shaped GFRP coating strengthening showed better performance on strength and ductility than normal reinforced concrete beams. Ali et al. (2021) stated that concerning the flexural reinforcement using CFRP (Carbon Fiber Reinforced Polymer) or GFRP in continuously reinforced concrete beams, two layers of CFRP and four layers of GFRP could strengthen as well as increase the stiffness of continuously reinforced concrete beams, respectively. Siswosukarto et al. (2024) reported similar results, observing that the application of additional GFRP layers led to notable enhancements in the stiffness and ductility of the material. In addition, there was research from Ogboin et al. (2021) on shear strengthening of reinforced concrete beams with different thicknesses of epoxy and GFRP. The specimen dimension in the finding was 100 mm $\times$ 150 mm of cross-section and 1100 mm span length. The results showed that externally coated GFRP could change the failure mode from brittle shear to flexural failure due to GFRP bonding. Another research was conducted by Gemi et al. (2021) on the flexural reinforcement of reinforced concrete beams using GFRP in the form of pultruded profiles, fabrics, and reinforcement. The finding showed that GFRP-covered beams could increase the beam's initial stiffness and load capacity. Research on reinforced concrete beams strengthened with CFRP and GFRP conducted by Saleem et al. (2019) explained that the failure pattern in beams reinforced with GFRP was in the form of rupture of GFRP sheets at the location of maximum tensile stress.

The review found that most of the research focused on strengthening reinforced concrete beams of a specific scaled size, resulting in improved beam strength. Notably, debonding failure is highly sensitive to scale effects, as smaller specimens often exhibit non-uniform FRP–concrete interface stresses, leading to premature failure before reaching maximum capacity, as reported by Nayak et al. (2018) and Saleem et al. (2019). These scale differences limit the representation of actual conditions and the generalization of results, highlighting the need for studies on full-size reinforced concrete beams. However, testing the flexural strengthening of full-size reinforced concrete beams with GFRP using the loading and unloading method is still limited. Therefore, research on full-scale beam sizes with loading-unloading needs to be performed. The theoretical analysis concerning the flexural strength of reinforced concrete beams with different numbers of GFRP layers also needs to be conducted to determine the approximate value of the flexural strength capacity based on the experiments for analysis. Therefore, conducting GFRP tensile tests with different numbers of layers is crucial for this analysis.

Hence, this research investigated the flexural strengthening of reinforced concrete beams with GFRP at full scale for moment-resisting system beams in the middle of the span, where the positive bending moments are dominant. In this region, the tensile zone is located at the soffit, which makes external GFRP installation more practical. Loading was performed in a loading-unloading process to investigate the behavior of flexural resistance and recovery. In addition, an analysis based on the theory of cross-sectional plasticity was also conducted to predict the strength value of the beam under loading. In flexural testing, the measured parameters consisted of stiffness, yield strength, ultimate load, mid-span deflection, ductility, and failure pattern. This research would be expected to achieve the significance of flexural stiffness and strength improvement, and influence the ductility of applying GFRP for structural strengthening.

2 METHODS

2.1 Specimen Details

The dimensions of the full-sized reinforced concrete beam were designed to full scale with a width of 200 mm, a height of 400 mm, and a span of 2200 mm. Following the process, the effective span of the beam for flexural testing was 1800 mm. The 1800 mm effective span is considered representative of actual structural conditions (ex., office building), as indicated by the calculated dead load (17.20 kN/m) and live load (7.2 kN/m). With the load combination of 1.2DL+1.6LL, the factored load is 32.16 kN/m. Thus, the corresponding ultimate moment is 13.03 kNm, and shear force is 28.95 kN, remaining below the section's flexural (40.25 kNm) and shear (120.05 kN) capacities, confirming a substantial safety margin.

The dimensions of the longitudinal reinforcement used amounted to two pieces with a diameter of 12 mm, each placed in the beam's tensile and compressive zones. The stirrup reinforcement dimension was 10 mm, with 100 mm apart for the support reinforcement and 200 mm apart for the midspan reinforcement, respectively. Relating to the measurements, the concrete cover measured 25 mm on all sides of the beam. Details of the size and reinforcement of the beam specimens are shown in Figure 1. Furthermore, according to the ACI 318M-14 standard, the calculated reinforcement ratio (ρ_{actual} = 0.30%) is slightly higher than the minimum

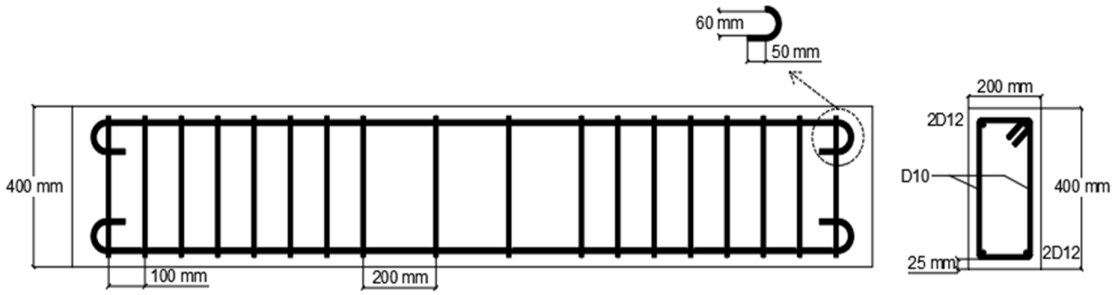

Figure 1. Beam specimen details.

requirement (ρ_{min} = 0.29%), yet still below the maximum allowable limit (0.75$\rho_{balance}$ = 1.69%) and sufficient tensile strain on the ultimate capacity (ε_{strain} = 0.044 > 0.005). Thus, the beam is categorized as under-reinforced, ensuring ductile behavior and providing the potential for additional tension reinforcement when the load needs to be increased due to upgrading the room function.

2.2 Material Properties

GFRP used an E-glass type with an effective thickness of 0.5 mm, having a unidirectional fiber direction. The polymer matrix used as GFRP binder was Epoxy resin Bisphenol-A-Epichlorohydrin mixed with Hardener-EPH 555 (Muflikhun and Fiedler, 2022). In this study, the uniaxial tensile tests of GFRP were conducted with four variations, i.e., one, two, three, and four layers of GFRP. These variations aimed to examine the mechanical behavior of GFRP associated with each configuration and provide reliable material properties for strengthening applications. GFRP tensile tests were conducted by forming 20 mm × 200 mm GFRP coupons with a resin and hardener mix ratio of 3:1. The number of coupons formed was three pieces for each number of layers. The method of producing GFRP coupons was the hand lay-up procedure. The tests were conducted based on ASTM (2014*b*). GFRP tensile test results are shown in Table 1 and Figure 3.

Based on these results, the average tensile strength and elastic modulus values used by GFRP were 7.3 MPa and 12.61 GPa. The results showed that in specimens where the number of GFRP layers increased, failure occurred due to looseness or slippage in the grip of the pulling tool, allowing the four-layer GFRP specimen not to reach its ultimate strength. Despite this limitation, the normalized tensile strength across different layer configurations remained relatively commensurate. This indicates that the objective of these tests was achieved, namely, to validate the applicability of single-layer properties for multi-layer laminates in strengthening applications. The GFRP damaged pattern during the process is shown in Figure 2.

The concrete used during the analysis had a compressive strength of 39.4 MPa. The tensile strength values of the main reinforcement and stirrups used were obtained from steel reinforcement tensile tests conducted based on ASTM (2014*a*). The reinforcement tensile test was conducted by taking samples from reinforced concrete beams after the beams had been tested for bending. Moreover, the reinforcement was obtained at the end of the beam that was not exposed to the support. The length of longitudinal reinforcement that was tensile tested was 400 mm. Meanwhile, the length of the stirrup reinforcement that was tensile tested was 300 mm. The number of reinforcement bars tested during the analysis was five. The tensile test results had an average value of f_y = 540.39 MPa and f_u = 736.02 MPa for longitudinal reinforcement. On the other hand, the average value of f_y = 623.37 MPa and f_u = 758.36 MPa for stirrup reinforcement.

2.3 Preparation of the Specimens

A total of five full-size reinforced concrete beams were used for flexural testing. Beam BL0 was the control beam without GFRP coating, and BL1 was coated with one layer of GFRP. Additionally, Beam BL2 was coated with two layers of GFRP, and three layers of GFRP were used for BL3. Following the process, Beam BL4 was coated with four layers during the analysis. GFRP layers were all located in the tensile fiber zone of the beam cross-section (bottom) along the span. The design details of the beam reinforcement with GFRP are shown in Table 2 and Figure 4.

2.4 Test Setup

Flexural testing was performed using a simple beam with a four-point bending test (Monier et al., 2017; Gemi et al., 2021; Hadi et al., 2022; Mirdan and Saleh, 2022). The load was placed at 1/3 and 2/3 of the effective span of the beam. During the process, the effective length of the beam tested was 1800 mm. The loading was conducted using a hydraulic jack whose load value was read by a load cell. LVDTs were placed at three points, one at the center of the beam span, and the

Table 1. Tensile strength results of GFRP per sheet

Material	Name	Tensile Strength (MPa)		
		Individual Results	Average values per layers	Modulus Elasticity (GPa)
GFRP 1 layer	1C	371.04	426.77	12.61
	1D	480.57		
	1F	413.95		
	1G	441.51		
GFRP 2 layers	2E	287.26	341.24	8.55
	2F	417.52		
	2G	318.93		
GFRP 3 layers	3E	318.56	363.10	7.77
	3F	387.46		
	3G	383.27		
GFRP 4 layers*	4E	188.37	200.68	4.83
	4F	196.33		
	4G	217.33		

*: Ultimate strength not achieved

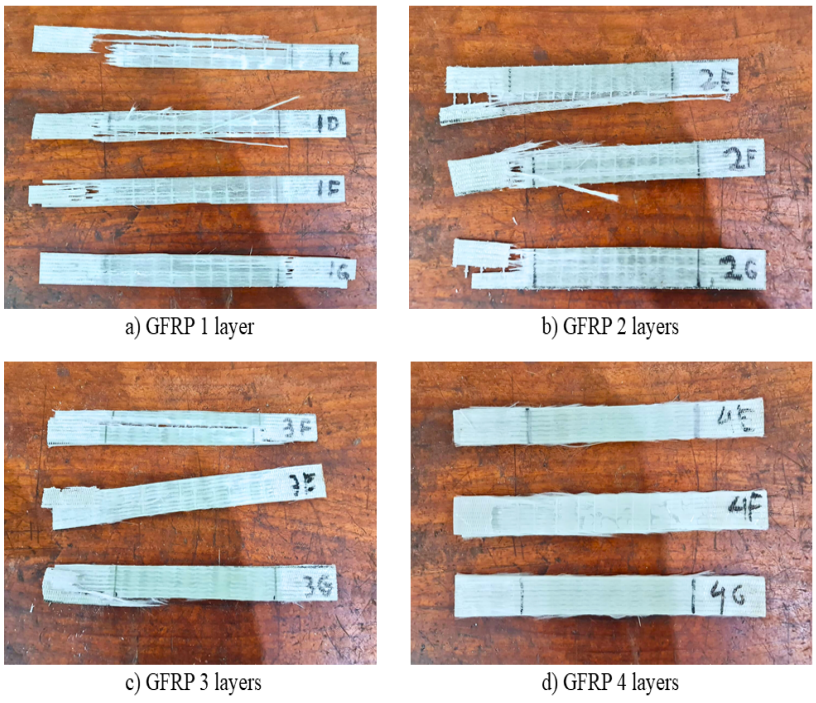

a) GFRP 1 layer b) GFRP 2 layers

c) GFRP 3 layers d) GFRP 4 layers

Figure 2. Experiment results of GFRP.

other two were positioned at 1/3 and 2/3 of the beam span to measure the deflection that occurred in the beam (Monier et al., 2017; Saleem et al., 2019). Moreover, the loading method was performed in a loading-unloading manner with a displacement interval of 0.6 mm. A data logger was installed to monitor the loading levels, deflection readings, and stresses generated by the beam. A schematic of the test setup in the analysis is shown in Figure 5.

In this research, the specimens were subjected to loading and unloading with an increment of 0.6 mm (0.1%

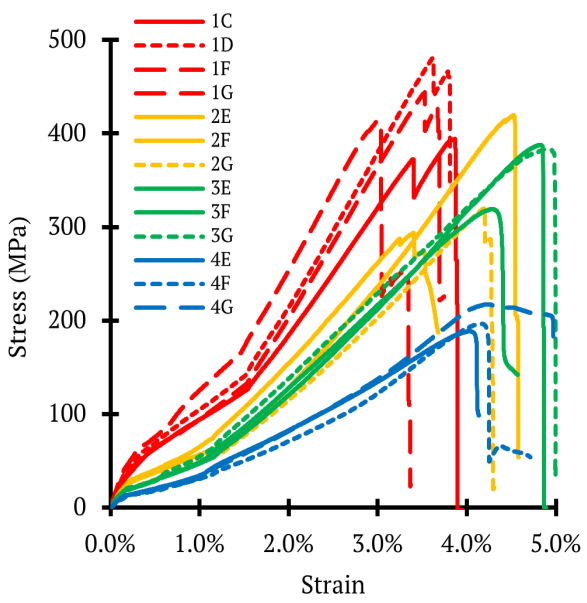

Figure 3. Stress-Strain of GFRP.

Table 2. Flexural test specimen variable details

Beam	Specimen Treatment	GFRP Position	Total Thickness of GFRP (mm)
BL0	Without GFRP	–	0
BL1	GFRP 1 layer	Tensile zone	0.5
BL2	GFRP 2 layers	Tensile zone	1.0
BL3	GFRP 3 layers	Tensile zone	1.5
BL4	GFRP 4 layers	Tensile zone	2.0

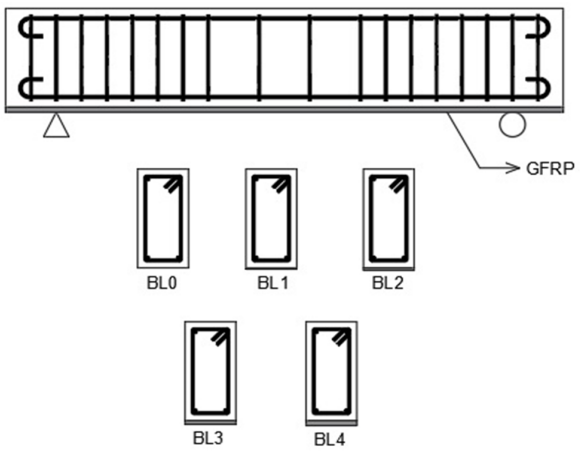

Figure 4. GFRP strengthening configurations for beam specimens.

of the 1/3 span length) until 30 mm (5% of the 1/3 span length). This range was established as a laboratory testing limit to capture both the initial response and the post-yield plastic behavior of the beam without causing premature failure. Although no formal code specifies the exact increment used in this study, similar displacement-controlled cyclic protocols have been reported in previous experimental research on RC beams (Zhu et al., 2022), in which fixed actuator displacement steps (e.g., 6 mm) were applied. The increment values differ, but the underlying principle of stepwise loading-unloading is comparable. The interval value was then increased to 2.4 mm (4 times 0.6 mm) for displacement values greater than 30 mm. The reason for adding the interval value was that when the displacement value reached the maximum deflection limit (5*L*/100), the beam being tested did not show any signs of failure.

2.5 Analytical Methods

The analysis method used to predict the flexural strength of full-size reinforced concrete beams was a theoretical analysis procedure and a fiber section analysis. The number of fiber sections used along the height of the beam section was 100 layers, with one section measuring 8 mm thick and 200 mm wide. In the context of this research, the theoretical analysis method was based on ACI Committee 318 (2014). It used Kent-Scott-Park (1980) theory to analyze concrete behavior in compressive conditions, especially through the post-peak behavior. However, the analytical calculation did not consider the occurrence of debonding between the GFRP and the RC beam surface. The modulus of elasticity used in this calculation resulted from a single-layer GFRP tensile test of 12.61 GPa. The tensile test result for the four-layer configuration was excluded because premature grip slip occurred, resulting in an unrealistically low modulus that does not represent the actual material property. Therefore, the modulus of elasticity (12.61 GPa) obtained from the single-layer GFRP tensile test was applied to all layer configurations by considering the number of layers through cumulative thickness, consistent with previous studies (Nayak et al., 2018; Saleem et al., 2019; Gemi et al., 2021). Concrete strain values were obtained with limits from 0.0001 to 0.035, having intervals of 0.0001. The concept of calculating the analytical flexural strength of reinforced concrete beams with GFRP was shown in Figure 6.

The reinforced concrete beams were subjected to flexural and shear forces induced by transverse loads. These shear forces generated significant shear stresses, particularly near the supports. The forces could lead to sudden brittle failure without earlier warning signs when not adequately resisted, such as deflection or flexural cracking. As a result, the shear capacity of the reinforced concrete beams was calculated to ensure

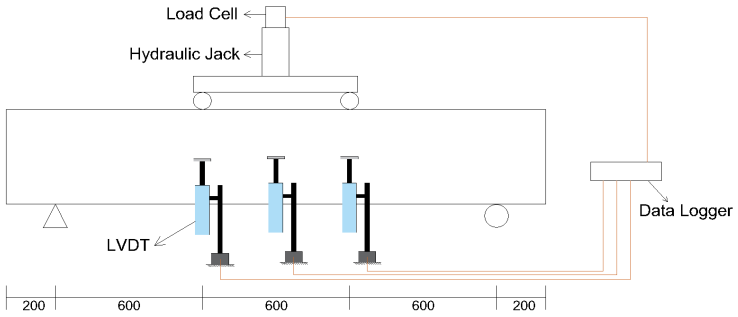

Figure 5. Test setup of the beam.

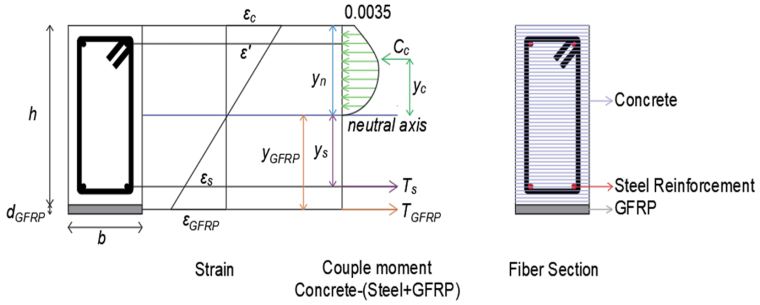

Figure 6. Concept of calculation of analytical flexural strength of reinforced concrete beams strengthened with GFRP.

that the beam did not experience brittle shear failure. The shear strength calculation was based on ACI Committee 318 (2014).

2.5.1 Calculation of the Beam Flexural Strength

The calculation of the flexural strength of the beam was conducted with the limitation of the plastic behavior of the reinforcing steel being elastic-perfectly plastic, with the values of f_y = 540.39 MPa, f_u = 736.02 MPa, and E = 200,000 MPa. The steps for calculating the flexural strength of the beam were as follows. The neutral axis was located in the concrete cover area or between the tensile and compressive reinforcement, where the strain conditions were considered producing and vice versa. When the axis was considered yielding, the tensile or compressive force was obtained by multiplying the area by the yield stress (f_y). However, when it was not producing, the tensile or compressive force was obtained from the multiplication of the area and the working stress (strain (ε) and the modulus of elasticity of concrete (E_c)).

The calculation of the analytical flexural strength of reinforced concrete beams due to the influence of GFRP was performed by adding the tensile strength value of GFRP, the area of GFRP sheets (A_{GFRP}), and the modulus of elasticity of GFRP (E_{GFRP}) into the flexural analysis calculation. The tensile forces were determined based on strain compatibility and the constitutive behavior of each material. The tensile force of reinforcing steel was calculated using an elasto-plastic model, where its stress was taken as (f_s). Meanwhile, the tensile force of GFRP was calculated assuming a linear behavior proportional to its strain and the elastic modulus. The stress is expressed as (f_{GFRP}). The stress of reinforcing steel in the elastic range is expressed in Equation (1), while the stress in the plastic range is expressed in Equation (2). For GFRP, the stress was assumed to behave linearly in proportion to its strain and elastic modulus, as expressed in Equation (3). Based on these stresses, the tensile force of reinforcing steel and GFRP were obtained using Equation (4) and Equation (5), respectively. The force equilibrium and moment equations used these forces and the concrete compression block (C_c) to determine the nominal flexural capacity.

$$f_s = \varepsilon_s \times E_s \tag{1}$$

$$f_s = f_y \tag{2}$$

where ε_s was the strain of the steel reinforcement and E_s is the elastic modulus of the steel reinforcement. For strain (ε_s) values less than the yield strength (f_y), the steel stress was determined using Equation (1), whereas for strain values greater than or equal to the yield strength, the steel stress was evaluated using Equation (2).

$$f_{GFRP} = \varepsilon_{GFRP} \times E_{GFRP} \tag{3}$$

$$T_s = A_s \times f_s \tag{4}$$

$$T_{GFRP} = A_{GFRP} \times f_{GFRP} \tag{5}$$

$$C_c = T_s + T_{GFRP} \tag{6}$$

where T_s signifies the tensile force of the reinforcement, A_s represents the area of tensile reinforcement, and T_{GFRP} is the tensile force of GFRP. Additionally, A_{GFRP} signified the area of GFRP (namely, the width of the beam times the thickness of the GFRP), f_{GFRP} is the tensile stress of GFRP, and C_c represents the concrete compressive force at equilibrium conditions. The calculation of the C_c value was based on the Kent-Scott-Park theory (Scott, 1980), where the Equation was as follows.

$$\sigma(\varepsilon) = f_c{}' \left[2\,\frac{\varepsilon}{\varepsilon_0} - \left(\frac{\varepsilon}{\varepsilon_0}\right)^2 \right] \tag{7}$$

$$C_c = \int_0^{y_n} b\,\sigma_{(\varepsilon)}\,dy \tag{8}$$

where ε_0 is the strain at maximum stress. The value of the strain at maximum stress for the elastic state is taken as $\varepsilon_0 \approx 0.002$ for the strain value $0 \leq \varepsilon \leq \varepsilon_0$. For softening state ($\varepsilon_0 < \varepsilon \leq \varepsilon_{cu}$), a linear descending branch is adopted until ε_{cu} (ultimate strain of concrete). The ultimate concrete strain's usual value is $\varepsilon_{cu} \approx 0.003$–$0.0035$.

The compressive and tensile strains were calsulated by assuming that the previous step produce the neutral axis depth from Equation (6). The results obtained were used to re-control the assumption of the neutral axis position and strain on the compressive reinforcement (ε') using Equation (9) and tensile reinforcement (ε_s and ε_{GFRP}) using Equation (10) and Equation (11).

$$\varepsilon' = \frac{y_n - d'}{y_n}\,0.0035 \tag{9}$$

$$\varepsilon_s = \frac{d - y_n}{y_n}\,0.0035 \tag{10}$$

$$\varepsilon_{GFRP} = \frac{d_{GFRP} - y_n}{y_n}\,0.0035 \tag{11}$$

where ε' are the compressive reinforcement strain, y_n signifies the depth of the neutral axis, and d' represents the distance from the farthest compression fiber to the center of the outermost layer of compression steel reinforcement. In addition, ε_s is the tensile strain, d signified the distance from the farthest compression fiber to the center of the outermost layer of tensile steel reinforcement, ε_{GFRP} was the strain of GFRP, and d_{GFRP} represented the distance from the farthest compression fiber to the center of the farthest GFRP layer.

The beam's nominal moment value (M_n) was calculated using the following Equation.

$$M_n = C_c\,y_c + T_s\,y_s + T_{GFRP}\,y_{GFRP} \tag{12}$$

where y_c was the distance from the extreme compression fiber to the centroid of the concrete compressive resultant C_c, y_s signified the distance of the outermost fiber of the tensile reinforcement to the neutral axis and y_{GFRP} represented the distance of the outermost fiber of the GFRP layer to the neutral axis.

2.5.2 Calculation of the Beam Shear Capacity

The calculation of shear capacity in reinforced concrete beams based on ACI Committee 318 (2014) was conducted as follows. First, the area of the stirrup reinforcement with Equation (13) was calculated. Second, the flexural shear capacity of concrete beams was calculated using Equation (14). Third, the flexural shear capacity of the stirrup reinforcement was calculated using Equation (15). Fourth, the ultimate shear capacity was calculated using Equation (16).

$$A_v = 2\left(0.25\pi d_s^2\right) \tag{13}$$

$$V_c = 0.17\lambda\sqrt{f_c{}'}\,b_w\,d \tag{14}$$

$$V_s = \frac{A_v f_{yv} d}{s} \tag{15}$$

$$V_u = (V_c + V_s) \tag{16}$$

Where A_v was the area of the stirrup reinforcement, d_s signified the diameter of the stirrup, and V_c represented the flexural shear capacity of concrete beams. Additionally, λ signified the factor of concrete type, f_c' was the compressive strength of the concrete, b_w represented the width of the beam, and d was the effective height of the beam. V_s represented the flexural shear capacity of the stirrup reinforcement, f_{yv} was the yield strength of the shear reinforcement, S signified the distance between stirrups, and V_u was the ultimate shear capacity.

3 RESULTS

3.1 Experimental Results

The results of experimental tests on reinforced concrete beams strengthened with GFRP are presented in this section. The data discussed included the load-displacement responses with residual forces and the behavioral stages of the reinforced concrete beams. Following the process, the load-displacement with residual forces of the beam section included the half hysteresis curve characteristic of each beam specimen. The stages of the behavior concerning the beam section

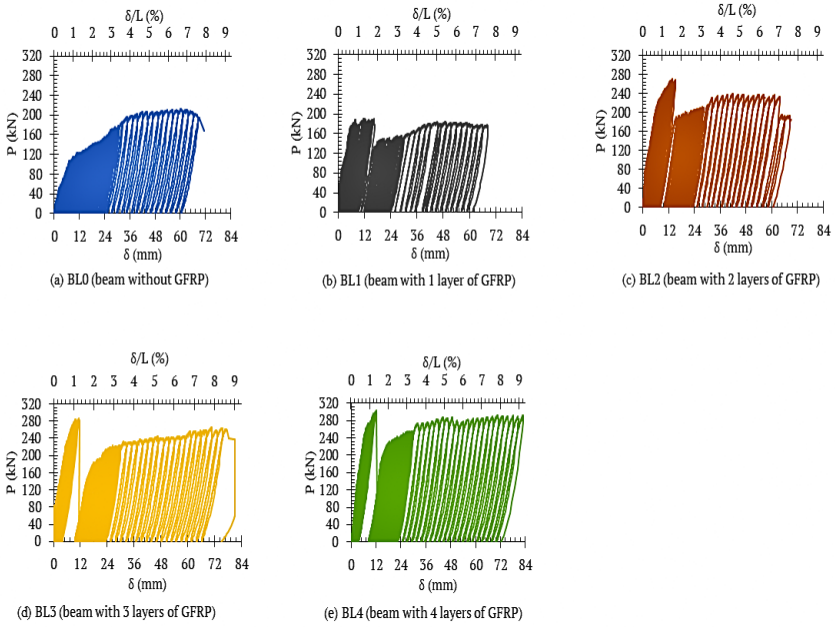

Figure 7. Load-displacement with residual forces of the beam.

contained the sequence of beam damage from the first crack to failure or collapse. The experimental results of load-displacement values with residual forces due to the loading-unloading method are shown in Figure 7. The review of the total experimental results, consisting of stiffness, displacement, force resistance, and ductility, is presented in Table 3 and Figure 8.

3.1.1 Load-displacement

The force-displacement curve of loading-unloading specimens in Figure 7 showed that all specimens exhibit a nearly linear stiffness during loading-unloading until the final state . According to the interpretation of the force-displacement curve in the Figure, there were some indications of stiffness and strength improvement because of strengthening with GFRP. In the same context, there was a change in the flexural resistance sequence.

Initial stiffness was a critical parameter that reflected the ability of a structural element to resist deformation under early-stage loading conditions. The results showed that the control beam (BL0), without any GFRP reinforcement, had the lowest stiffness value of 20,750 N/mm. Applying a single GFRP layer (BL1) significantly increased the stiffness to 42,500 N/mm, while BL2 and BL3 achieved 46,670 N/mm and 63,170 N/mm, respectively. Further increase in GFRP layers to four (BL4) led to a reduced stiffness of 46,000 N/mm, signifying a potential inefficiency due to excessive layer thickness, which caused premature debonding or uneven stress distribution. This trend was shown in the load-displacement hysteresis curves in Figure 7. The curve of BL0 showed the most gradual initial slope, signifying low stiffness, while BL3 indicated the steepest initial slope, correlating with its highest calculated stiffness. BL1 and BL2 showed a progressive increase in stiffness with distinctively steeper initial curves than BL0. On the other hand, as BL4 showed a relatively high load-carrying capacity, the initial stiffness was lower compared to BL3, confirming that additional layers did not necessarily contribute to a proportional increase in stiffness.

The specimens with additional GFRP strengthening showed significant flexural strength improvement in elastic to early plastic deformation. A momentary loss in flexural resistance occurred due to 1.2% to 2.0% of flexural deformation. After the debonding occurrence, which momentarily activated a drop in flexural resistance, the flexural resistance rose to achieve the second ultimate strength at 4.7% to 7.9% of flexural deformation. This sequence of resistance mechanisms generated two peaks of flexural strength, which were named the first and second ultimate flexural strength, respectively. In comparison, the unstrengthened specimen (BL0) demonstrated a more gradual increase in resistance after yielding, attaining its ultimate strength at a flexural deformation of 6.3%, before softening led to failure. There was an exception in one-layer GFRP-strengthened specimens (BL1); the second ultimate flexural strength did not achieve the ultimate strength of the unstrengthened specimen (BL0). Thus, two ultimate flexural strengths in the strengthened beams

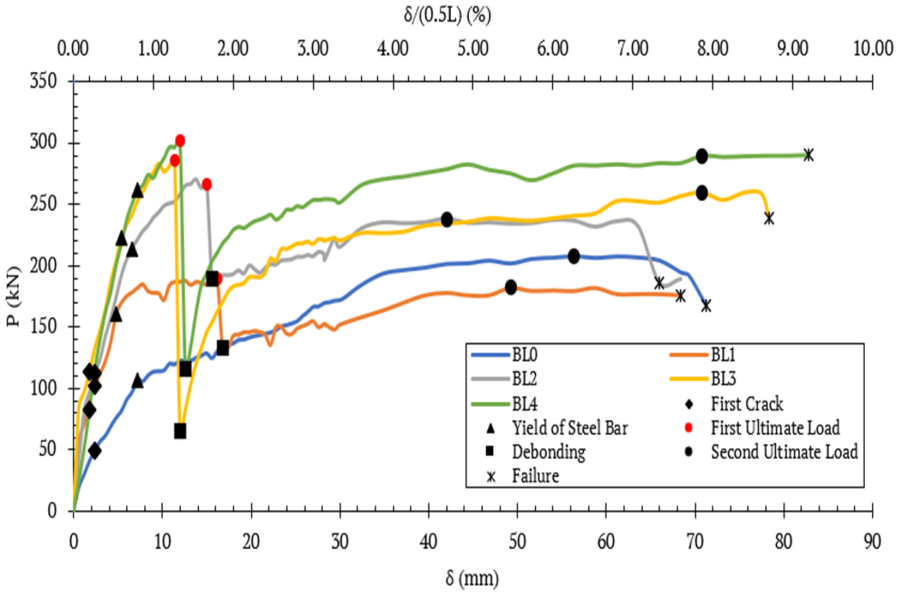

Figure 8. Load-displacement of the beams test result.

also corresponded to developing two distinct ductility states.

The ductility evaluation at both debonding (1^{st} ductility) and ultimate stages (2^{nd} ductility) further clarified this behavior. Based on Table 3, BL1 and BL2 exhibited relatively close ductility values. This indicates that the occurrence of debonding did not immediately terminate their deformability. In contrast, BL3 and BL4 presented a significant momentary loss of bending moment resistance once debonding occurred. Nevertheless, the flexural resistance recovered and increased until reaching the second ultimate state, and this increase demonstrated that the strengthened beams were still able to preserve greater resistance and deformability compared to the unstrengthened beam.

3.1.2 Behavior of Reinforced Concrete Beam Under Incremental Loading

The reinforced concrete beam behavior stages comprised the first crack, yielding, ultimate, and last failure. The experimental load and displacement values for all stages of behavior concerning all reinforced concrete beam specimens are shown in Table 3 and Figure 8. In line with the analysis, the initial stage in reinforced concrete beams due to loading was the appearance of the first crack. In the beam with one layer of GFRP (BL1) and two layers (BL2) in the beam without GFRP (BL0), the first crack occurred at a displacement of 2.4 mm. Relating to the process, the first crack occurred at a displacement of 1.8 mm in the beam with three and four layers.

Table 3. Summary of the beam test results

Beam	Initial Stiffness (N/mm)	First Crack		Yield		Debonding of GFRP		1^{st} Ultimate Load		2^{nd} Ultimate Load		Failure		Ductility (μ)	
		Load (kN)	Disp. (mm)	Load (kN)	Disp. (mm)	Load (kN)	Disp. (mm)	Load (kN)	Disp. (mm)	Load (kN)	Disp. (mm)	Load (kN)	Disp. (mm)	1^{st}	2^{nd}
BL0	20,750	49.8	2.4	107	7.2	–	–	–	–	208.3	56.4	168.09	71.21	–	9.89
BL1	42,500	102	2.4	160.5	4.8	133	16.8	189	16.2	182	49.2	176	68.4	3.38	14.25
BL2	46,666.67	112	2.4	214	6.6	190	15.6	267	15	238.2	42	186	66	2.27	10
BL3	63,166.67	113.7	1.8	223	5.4	65	12	286	11.4	260	70.8	239.3	78.39	2.11	14.52
BL4	46,000	82.8	1.8	262	7.2	116	12.6	302	12	290	70.8	290.5	82.8	1.67	11.5

The yielding of the beam reinforcement occurred after the first crack of the concrete beam specimens. The yield deformation in all beams was 4.8 - 7.2 mm, as shown in Table 3 and Figure 8. The lowest load value when yielding was in beam BL0 of 107 kN, while the highest was in BL4 of 262 kN. This showed a rise in the yield strength value along with the increase in the number of GFRP layers. In the research context, the debonding of the GFRP layer and concrete surfaces was observed under a slightly increased load. GFRP debonding started with a horizontal crack in the middle span of the beam, which then spread to a more peripheral area, as similarly observed in the research by Hijriah et al. (2019). Figure 10 shows the beam damage pattern when GFRP debonding occurred in BL1, BL2, BL3, and BL4.

Figure 9 shows the crack pattern and debonding formation of the beams at GFRP debonding phase. The classification of beam failure modes presented in Figure 9 refers to ACI 318-11 (ACI Committee 318, 2011). Initial debonding of the interface between GFRP and concrete was observed at a displacement of 7.2 mm under a load of 182 kN in BL1 specimens. Despite the onset of the interface GFRP and concrete cracking, the load continued to increase, reaching the first peak load of 189 kN at a displacement of 16.2 mm. Subsequently, GFRP debonding occurred in the beam at a displacement of 16.8 mm, accompanied by a load reduction to 133 kN, representing a 29.63% decrease. The load recorded at the onset of debonding was equivalent to the load observed in the control beam at an identical displacement. The damage pattern on each beam strengthened with GFRP when GFRP debonding occurred, as shown in Figure 9. Beam BL1 showed prominent ver-

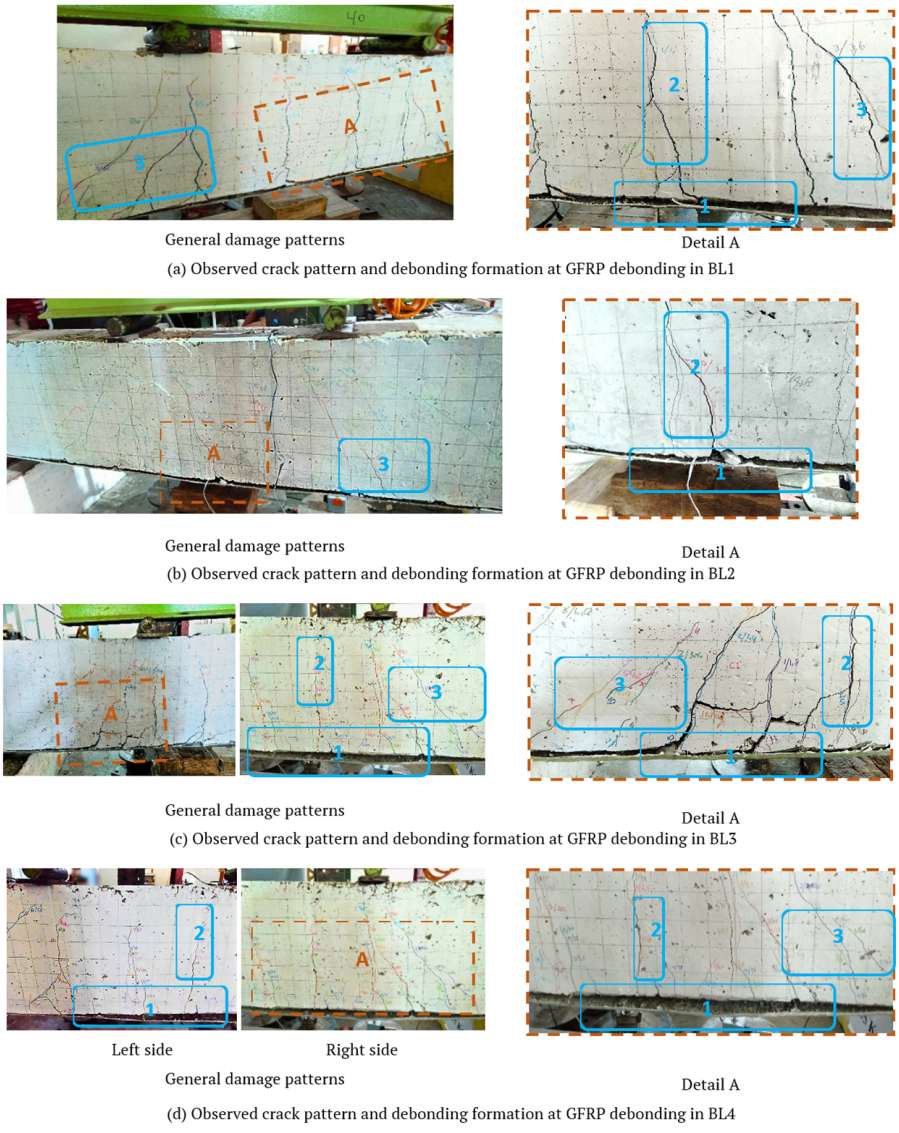

Figure 9. Debonding of GFRP on the beam.

*) 1 is GFRP debonding damage, 2 is flexural crack, and 3 is flexural–shear crack.

tical and diagonal cracks progressing from the bottom to the top fiber, primarily focused at mid-span, where the flexural load was the highest. Moreover, GFRP debonding showed that the applied load exceeded the bond strength between GFRP and the concrete surface. Debonding was typically initiated at the GFRP end and propagated inward, accompanied by flexural and shear cracks, indicating the failure of the external reinforcement in resisting tensile stress in the lower zone of the beam.

The debonding of the GFRP interface for beam BL2 was initiated at a displacement of 10.8 mm under a load of 250.5 kN. Despite the progressive cracking of the interface, the load-bearing capacity continued to increase, reaching an ultimate load of 267 kN at 15 mm displacement. This was followed by GFRP debonding at 15.6 mm, leading to a load drop to 190 kN, corresponding to a 28.84% reduction. Beam BL2 showed less severe flexural damage than BL1, with vertical cracks at mid-span and minimal diagonal cracking, as shown in Figure 9. GFRP debonding was more limited, possibly due to effective stress distribution in the early loading phase. After the bond strength was exceeded, the GFRP started to detach gradually, signifying that while GFRP improved flexural strength, its effectiveness diminished when adhesive failure occurred.

GFRP interface in beam BL3 started to detach at a displacement of 9.6 mm when the applied load reached 283.6 kN. Despite the continued cracking along the interface, the beam could sustain an increased load until its first ultimate at 286 kN at 11.4 mm. After the process, debonding of the GFRP interface occurred, leading to a drastic load reduction to 65 kN at 12 mm, equivalent to a 77.27% decrease. This pronounced loss in capacity was possibly associated with irregularities in the concrete, potentially due to inadequate mixing or inconsistent placement during casting. According to Figure 9, the beam BL3 showed extensive cracking in vertical, diagonal, and horizontal directions, implying severe structural damage. GFRP interface showed clear debonding, marking the failure of the reinforcement system. As the concrete surface debonded, GFRP lost its ability to resist tensile forces, allowing cracks to propagate freely. This showed the loss of flexural strength improvement due to the breakdown of the bond between concrete and reinforcement.

Beam specimen BL4 showed the initial release of GFRP interface at a displacement of 6.6 mm under a load of 250.9 kN. Despite progressive interface cracking, the load-carrying capacity rose, reaching the first ultimate load of 302 kN at 12 mm displacement. However, the occurrence of GFRP interface debonding shortly afterward caused a significant reduction in load to 116 kN at 12.6 mm, marking a 61.59% decrease. Beam BL4, as shown in Figure 9, showed the least severe cracking, with a few diagonal cracks forming but not propagating. Following the discussion, GFRP remained effective in resisting tensile forces, allowing the beam to retain its structural integrity longer than the others.

After GFRP debonding, beams BL1, BL2, BL3, and BL4 could still withstand the load until the components reached the second ultimate load. GFRP, having the second ultimate load on beams, was higher than that without GFRP, even though the beams with the polymer had experienced debonding. In beam BL1, the ultimate load value was 12.63% lower than BL0. Meanwhile, the ultimate load value was greater than that of the control beam in beams BL2, BL3, and BL4, which were 14.35, 24.82, and 39.22%, respectively. These results showed that despite the occurrence of debonding, GFRP still contributed to improving the residual load-bearing capacity of the beams.

Figure 8 showed that the strength of each beam started to decline due to failure mechanisms after reaching the second ultimate load. In beam BL0, failure occurred due to the rupture of the longitudinal reinforcement, signifying a typical tensile failure. Beam BL1 did not collapse but stopped due to signs of compression failure. Similarly, beam BL2 showed a load drop of 19.83% (from 232 kN to 186 kN) at a displacement of 66 mm, followed by a slight increase of 0.016% (to 189

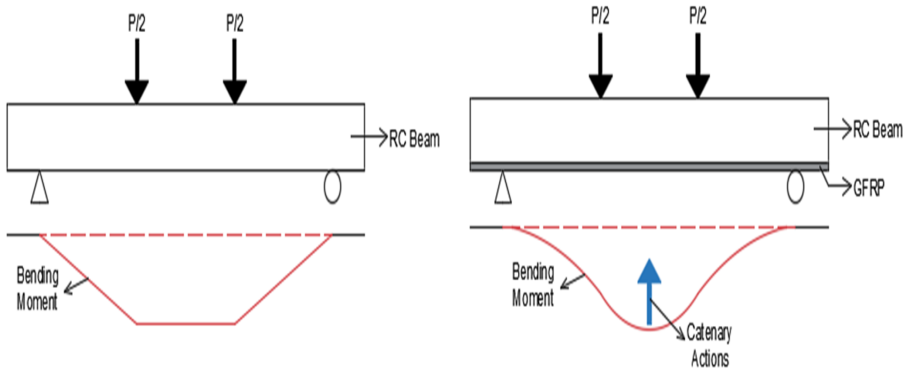

Figure 10. Schematic of the difference between normal bending moment and bending moment accompanied by catenary actions on RC beams.

kN at 68.4 mm), leading to termination of the test even though collapse had not occurred. Beam BL3 reached collapse at a displacement of 78.39 mm under a load of 239.3 kN, marking a complete structural failure. Conversely, beam BL4 showed compression failure without collapse and indicated overstrength behavior, as no load reduction occurred from the peak load until the test was stopped.

4 DISCUSSION

This section discusses stiffness and load on the first crack, load of yielding steel reinforcement, debonding of GFRP, first and second ultimate loads, beam failure modes, and ductility. It also discussed comparing experimental results and analytical outcomes for each beam specimen.

4.1 Stiffness

The stiffness is defined as the ability of a structural element to withstand deformation when subjected to a force. Quantitatively, it is expressed as the ratio between the applied force and the resulting displacement (Gere and Goodno, 2012; Beer et al., 2015). The stiffness in the first crack values is shown in Table 3. The results showed that adding GFRP layers generally increased the stiffness of the beam BL1 104.82%, BL2 124.90%, BL3 204.42%, and BL4 121.69% compared to the normal beam (BL0). BL3, the beam with three layers of GFRP, achieved the highest stiffness. This showed that the configuration was the most effective in increasing the initial resistance to deformation. However, in BL4 (beam with four layers of GFRP), the stiffness was 27.18% lower than in BL3. The observed decrease in initial (elastic) stiffness in BL4 could be attributed to several interrelated structural and material phenomena despite adding a fourth GFRP layer. An imperfection in the RC beam specimen or the GFRP layer bonding process may cause this anomaly.

4.2 First Crack

According to Table 3, including a strengthened beam with GFRP generally increased the first crack load compared with the control beam, indicating that the additional tensile capacity from GFRP delayed the onset of cracking. However, in the case of BL4, which contained the largest GFRP area, the first crack load is lower than that of BL2 and BL3. This non-monotonic trend suggests that beyond a certain reinforcement ratio, the relatively low modulus of elasticity of GFRP may alter the strain distribution and transfer higher localized tensile stress to the concrete, thereby accelerating the crack initiation. Since concrete is inherently weak in tension, once the tensile strain exceeds the concrete's limit, cracking can significantly diminish its tensile and shear strength, accelerating structural degradation in that region (Araby et al., 2021). Although this early cracking does not immediately compromise the ultimate capacity, it may trigger progressive damage under cyclic or increasing loading conditions, emphasizing the importance of balancing reinforcement ratio, stiffness compatibility, and bond characteristics in designing GFRP-strengthened beams.

4.3 Yield Strength

According to Figure 8, adding GFRP layers significantly improved the yield strength of the beams. Compared to beam BL0, the yield strength increased by 50% in BL1, 100% in BL2, 108.41% in BL3, and 144.86% in BL4, respectively. Based on the experimental results in Table 3, an additional GFRP layer for strengthening the beam increased the load resistance to the yield state.

4.4 Debonding of GFRP

Based on the backbone curve monitoring, the load resistance of all strengthened beams with GFRP suddenly dropped shortly after debonding, with load resistance contiguous to the backbone curve of BL0. In the case of the BL1 specimen, even though the initial strength was higher compared to control RC beams, strengthening the beam with only one layer of GFRP did not enhance strength after debonding to the ultimate state. In the BL2 specimens, the load resistance after GFRP debonding until the ultimate state occurred was higher than that of the control RC beam. The lowest load resistance when debonding occurred was in the BL3 beam. However, after the debonding occurrence to the ultimate state, the load resistance was increased with a slightly larger magnitude than the BL2. With the same pattern of backbone characteristics as BL3, BL4 achieves larger load resistance than BL3 in its ultimate state.

4.5 Ultimate Load

Based on the experiment results, two ultimate loads occurred, namely before (the first ultimate load) and after the debonding of GFRP (the second ultimate load). The first ultimate loads from the beams BL1, BL2, BL3, and BL4 were higher than those of BL0 (without GFRP). This showed that the additional layers of GFRP increased the strength capacity of the beam. GFRP in the tensile zone contributed to withstanding the flexural stress, reducing the load borne by the steel reinforcement. The presence of GFRP also allowed the stress distribution between concrete, steel, and GFRP to be more balanced.

Following GFRP debonding, the second ultimate load decreased relative to the first ultimate load by 3.7% in beam BL1, 10.79% in beam BL2, 9.09% in beam BL3, and 3.97% in beam BL4, respectively. However, these beams' second ultimate load value was higher than that of the beam without GFRP, except for beam BL1. The outcome could occur due to the non-uniformity of the concrete material in the BL1 beam, signifying that its ultimate strength could not exceed BL0.

The increase in the second ultimate load observed in beams reinforced with two, three, and four layers of GFRP showed that such strengthening significantly improved the load-bearing capacity of the beam compared to the unstrengthened beam. This improvement was attributed to the catenary action of the detached GFRP in the plastic hinge region, where the polymer behaved similarly to a tension tie that bridged the cracked concrete and redistributed tensile forces (Palanivel and Sekar, 2013). After debonding, GFRP contributed to load resistance by developing membrane forces, which delayed further structural degradation. This showed the effectiveness of the polymer in increasing tensile strength and improving stress distribution across the beam, maintaining structural performance after interface failure. The schematic of the difference between the normal bending moment and that accompanied by catenary actions on RC beams is shown in Figure 10.

4.6 Failure Mode

In the BL0 specimen, the failure observed was the breakage of the reinforcing steel in the middle of the span, and the compression fibers were crushed. Figure 11 shows the beam damage pattern at failure during the experimental testing. The beam failure modes' classification refers to ACI 318-11 (ACI Committee 318, 2011). This beam experienced severe failure with wide cracks in the middle of the bottom that spread upward. The lack of additional reinforcement allowed cracks to develop rapidly on the concentrated middle zone of the beam, leading to complete failure.

In the BL1 specimen, the failure pattern was the combination of slight crushing compression failure of concrete and large tension cracking accompanied by spalling of concrete. The main crack still appeared in the center, but looked narrower and more controlled than BL0. The single layer of GFRP withstands the tensile force but is inadequate to prevent large cracks from forming. Moreover, the crack pattern was flexural (2) and flexural-shear (3).

According to Figure 12, beam specimen BL2 had greater cracks but appeared smoother and more widespread. Localized concrete crushing and spalling on the compression fiber initiated the failure.

In the final failure, the deformed shape, the shear deformation in the inclined wide crack line bridging the compression crushing, and the largest tension cracking zone were observed. The failure pattern observed in beam BL3 showed clear signs of delamination of GFRP layers, with the wide concrete cracking and disintegrated spalling formation of the tensile zone concrete cover. It was also accompanied by localized spalling and crushing in the compression zone. The vertical wide cracks formed in the final loading, bridging the spalled compression crushing zone to the tension disintegrating zone.

The failure mode in beam BL4 showed that distributed compression crushing damage occurred along the designed plastic hinge. Despite the compression failure, the smoother tension cracks were distributed along the designed plastic hinge zone.

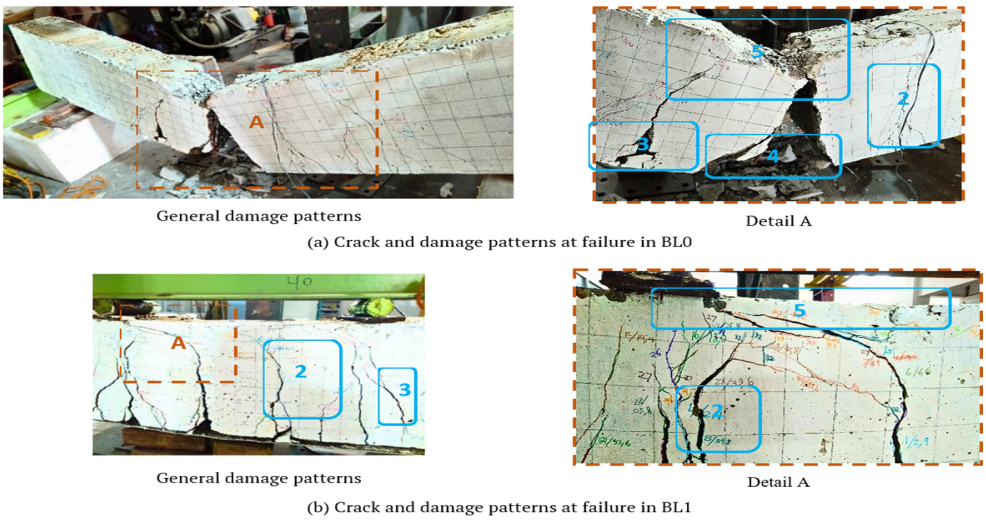

Figure 11. Failure modes of the beams BL0 and BL1.

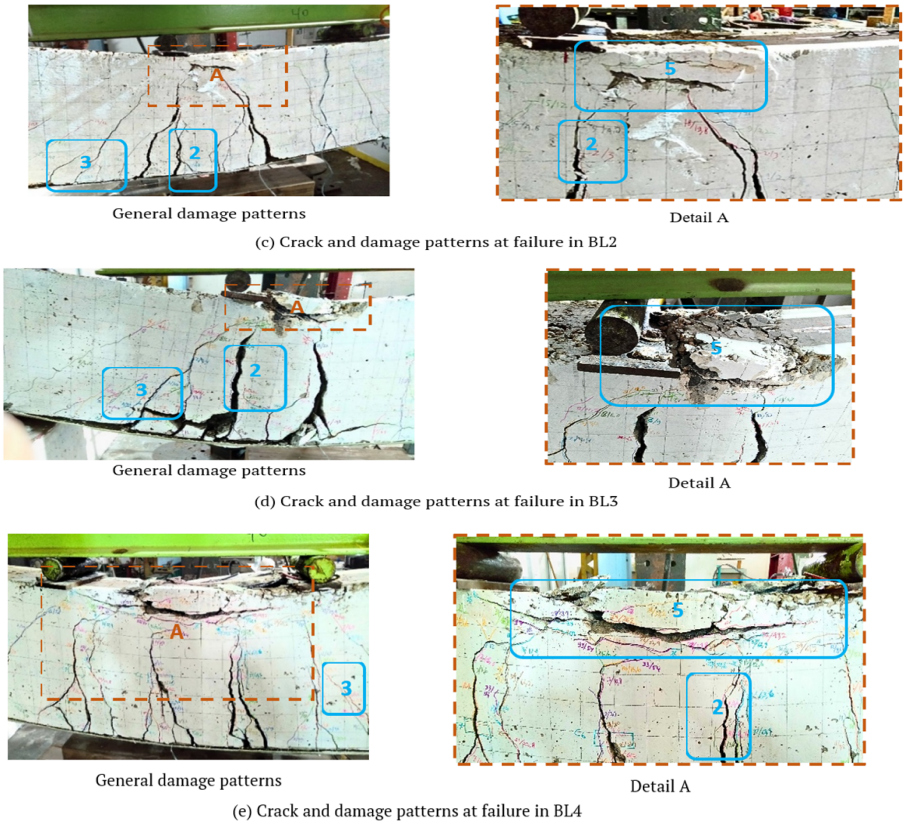

Figure 12. Failure modes of the beams BL2, BL3 and BL4.

*) 1 is GFRP debonding damage, 2 is flexural crack, 3 is flexural-shear crack, 4 is tensile steel rupture, and 5 is compression concrete crushed.

In the failure state, even though BL2, BL3, and BL4 beams had experienced crushing damage on the compression fiber, the tension cracking of the strengthened beam specimens was more distributed than that of the control specimens. The tension cracks, i.e., flexural and flexural-shear cracks, grew and widened, preceding the failure occurrence. Meanwhile, the difference in damage location of the compression and tension zone generated a difference in the crack pattern. This distribution of cracks indicates a more ductile failure mechanism, where energy is gradually dissipated through multiple cracking zones rather than concentrated at a single failure point.

4.7 Ductility

Ductility is the ability of a structure to experience large deformation after yielding without significant loss of strength (Paulay and Priestley, 1992). This feature could be calculated by the ratio of ultimate displacement to displacement when yielding (Priestley et al., 2007). The results of the ductility calculation in this analysis are shown in Table 3. Based on Table 3, beam BL0 showed the lowest ductility value among all specimens. The highest ductility was observed in beam BL3, which implied an increase of 46.78% compared to BL0, followed by a 44.08% BL1 increase, 16.28%, BL4, and BL2 with only a 1.11% improvement. These results signified that adding one and three layers of GFRP effectively improved the beam's strength and deformation capacity, allowing a wider plastic response before failure.

Despite beam BL3 having more GFRP layers than BL2, and being expected to be stiffer, its ductility was significantly higher. This was attributed to more effective crack distribution, increased concrete strength due to enhanced restraining action (Siswosukarto et al., 2024), better bonding performance, and the contribution of catenary action from GFRP after debonding. For beam BL4, the ductility was lower by 20.78% compared to BL3, which used four layers of GFRP, but still higher by 15% than BL2. This lower value was attributed to the increased stiffness from excessive GFRP layering, which restricted plastic deformation and led to a more brittle failure behavior.

The findings suggest that GFRP strengthening generally helps maintain or improve ductility, but the optimal number of layers is critical to prevent overstiffening and preserve plastic deformability. The distinction between ductility at debonding (first ductility) and at the ultimate stage (second ductility) fur-

ther clarifies this behavior. While the beams with one and two layers exhibited relatively consistent values between the first and second ductility, the beams with three and four layers experienced a momentary reduction at the first ductility, indicating a brittle response caused by the momentary loss of flexural capacity after debonding. However, the recovery of strength through catenary action resulted in a higher second ductility, which explains the overall improvement observed in BL3. This higher ductility also demonstrated that the strengthened beams still preserved greater resistance and deformability compared to the unstrengthened beam. Since the beams in this study were designed as gravity load–carrying members rather than for seismic applications, the obtained ductility can be considered adequate as long as no immediate strength degradation occurs after yielding of steel reinforcement.

4.8 Comparison of Experimental Results and Analytical Results

Compared to the analytical ultimate flexural strength (P, M_n anl.), the experimental specimen of BL0 showed a slightly larger strength. The discrepancy might be that the analytical approach did not consider the strain-hardening behavior of the reinforcing steel. The tensile test results of the steel reinforcement used in this study (presented in the material properties subsection) confirmed strain-hardening up to the ultimate strength (f_u). However, to simplify the analytical model, the steel behavior is idealized as perfectly elasto–plastic, using the measured yield strength (f_y) as the yielding plateau. This assumption is common in flexural strength analysis and may explain the slight underestimation of analytical results compared to the experiment. In real conditions, reinforcing steel could achieve strain hardening in the range of 1.25 to 1.5 (Andriono and Park, 1986; ACI Committee 318, 2014). The theoretical shear strength of the specimen, according to ACI Committee 318 (2014), includes considering the resistance contribution of both concrete shear (V_c) and steel stirrups (V_s) symbolized as P, V_n ACI 318-14. The comparison of the ultimate strength values between the experimental results and the analysis is shown in the backbone curves of Figure 13. The shear strength calculation is used to ensure that the beam remains on the ductile behavior (flexural failure than shear failure).

Reinforced concrete beams are generally susceptible to two brittle failure modes: (1) concrete compression failure under flexure and (2) shear failure. Figure 13 presents two control limits to address these aspects: (a) analytical flexural strength and (b) shear strength based on ACI 318-14. In the ultimate state, the analytical results showed that the strain of GFRP layers was 0.042 (1 layer), 0.039 (2 layers), 0.036 (3 layers), and 0.033 (4 layers), respectively. These strain values confirm that the beams with 1-4 layers of GFRP exhibited ductile behavior (ε_{strain} > 0.005). On the other hand, according to the shear strength control, the capacities of the beams with 1-4 layers of GFRP were lower than their analytical flexural strengths (P, M_n anl.). Consequently, if the ultimate flexural strength were to be exceeded, the beams would be expected to undergo shear failure. Nevertheless, in the experimental results, beams with 1-4 layers of GFRP experienced debonding, preventing them from reaching their analytical ultimate flexural strengths. Furthermore, Figure 13 includes the shear strength of the beams to ver-

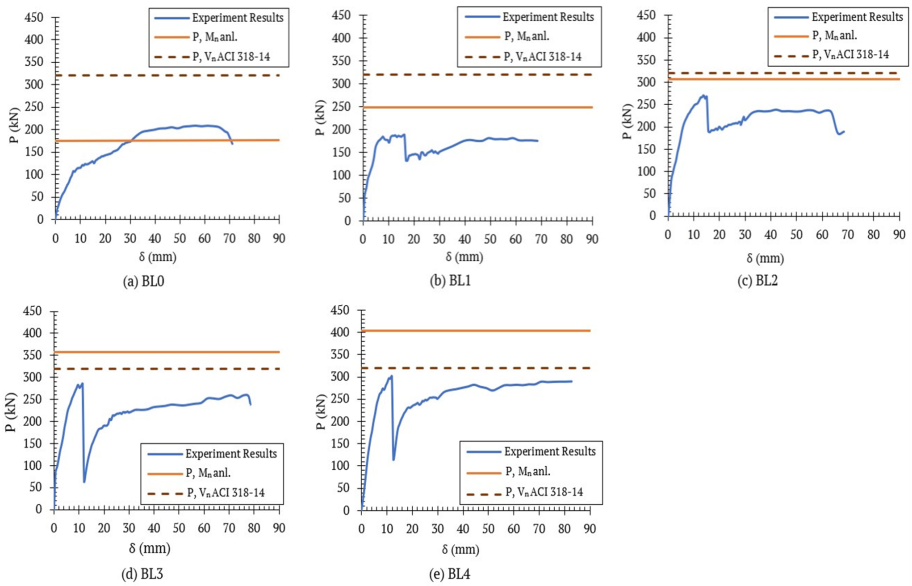

Figure 13. Load-displacement of the experiment and analytical result.

ify that the flexural strength of the GFRP-strengthened beams remains lower than their shear capacity (P, V_n ACI 318-14). This condition ensures that the beams predominantly exhibit ductile behavior.

Nevertheless, all beams strengthened with GFRP showed less ultimate flexural strength than the theoretical strength, as shown in Figure 13. The reason is the contribution of GFRP in enhancing flexural strength with composite section action only before the occurrence. After debonding occurred, the composite action of GFRP with the RC beam section was no longer effective. The GFRP only contributed support to the beam moment resistance with catenary action.

5 CONCLUSION

In conclusion, the results of the experimental analysis of full-scale reinforced concrete beams with GFRP were as follows.

a Adding GFRP layers increased the flexural elastic stiffness of the strengthened concrete beams, improving resistance to deformation before cracking. The results showed that adding GFRP layers increased the elastic stiffness of the beam BL1 by 104.82%, BL2 by 124.90%, BL3 by 204.42%, and BL4 by 121.69% compared to the normal beam (BL0).

b The use of GFRP layers considerably improved the yield strength of the beams. Yield strength increased by 50% BL1, 100% BL2, 108.41% BL3, and 144.86% BL4 compared to the unstrengthened beam (BL0). These results signified that beams strengthened with GFRP achieved higher load resistance before the internal steel reinforcement reached the yield point.

c The beam with two to four layers of GFRP still showed the second ultimate flexural strength improvement, ranging from 14.35% to 39.22%, compared to the unstrengthened beam. This signified the effectiveness of the polymer in increasing ultimate flexural strength.

d The application of GFRP strengthening generally contributed to preserving the ductility performance of beams at the second ultimate flexural stage. During the analysis, BL3 and BL4 specimens enhanced second ductility (ductility values at the ultimate state). However, when observed from the first ductility (ductility values at the debonding state), a reduction was evident due to the momentary loss of bending moment resistance at debonding. Even so, the second ductility demonstrated that the strengthened beams could still preserve greater resistance and deformability compared to the unstrengthened beam.

e All beam specimens reinforced with GFRP signified debonding, with variations in displacement and corresponding load reduction. However, most of the specimens maintained the ability to sustain additional loading past the point of debonding. Despite debonding initiated near the midspan, GFRP remained effectively attached outside the central one-third span, enabling it to continue providing tensile resistance as catenary action. Consequently, two peak ultimate load stages were observed before and after the onset of GFRP debonding.

f The analytical model used to estimate the ultimate flexural load tended to slightly exceed the experimental results, particularly for beams strengthened with two or more layers of GFRP. This discrepancy arose because the theoretical calculations did not consider the debonding between GFRP and the concrete surface of the RC beam, leading to an overestimation of the ultimate flexural load compared to the experimental results.

g Despite the addition of GFRP layers tending to increase strength and preserve ductility, there were indications that increased stiffness could limit plastic deformation. For configurations using more than four layers of GFRP, careful consideration should be performed to maintain equilibrium between the tensile and compressive zones to prevent premature brittle failure in the compression region of concrete.

DISCLAIMER

The authors declare no conflict of interest.

ACKNOWLEDGMENTS

The authors are grateful to the Heads of Structural Laboratory, Heads of the Materials Laboratory, Department of Civil and Environmental Engineering, and the Head of the Materials Laboratory, Department of Mechanical and Industrial Engineering, for the assistance and facilities provided during the specimen preparation and testing phases.

REFERENCES

ACI Committee 318 (2011), *Building Code Requirements for Structural Concrete (ACI 318-11) and Commentary*, American Concrete Institute, Farmington Hills, Michigan, USA.

ACI Committee 318 (2014), *Building Code Requirements for Structural Concrete (ACI 318-14) and Commentary (ACI 318R-14)*, 1 edn, American Concrete Institute, Farmington Hills, MI.

ACI Committee 440 (2006), *Guide for the Design and Construction of Concrete Reinforced with FRP Bars (ACI 440.1R-06)*.
URL: *https://www.concrete.org/*

Ali, H., Assih, J. and Li, A. (2021), 'Flexural capacity of continuous reinforced concrete beams strengthened or repaired by cfrp/gfrp sheets', *International Journal of Adhesion and Adhesives* **104**.
URL: *https://doi.org/10.1016/j.ijadhadh.2020.102759*

American Concrete Institute (2017), *Guide for the Design and Construction of Externally Bonded FRP Systems for Strengthening Concrete Structures*, American Concrete Institute, Farmington Hills.

Andriono, T. and Park, R. (1986), 'Seismic design considerations of the properties of new zealand manufactured steel reinforcing bars', *Bulletin of the New Zealand National Society for Earthquake Engineering* **19**(3), 213–246.
URL: *https://doi.org/10.5459/bnzsee.19.3.213-246*

Araby, Z., Rizal, S. A. and Afifuddin, M. (2021), 'The analysis of beam-column joint reinforced with cross bars according to sk sni t-15-1991-03 on cyclic loads', *Journal of the Civil Engineering Forum* **8**, 1–10.
URL: *https://doi.org/10.22146/jcef.3601*

ASTM (2014*a*), *A370: Standard Test Methods and Definitions for Mechanical Testing of Steel Products*.

ASTM (2014*b*), *Standard Test Method for Tensile Properties of Polymer Matrix Composite Materials (ASTM D3039/D3039M)*.
URL: *https://doi.org/10.1520/D3039*

Beer, F. P., Johnston Jr., E. R., DeWolf, J. T. and Mazurek, D. F. (2015), *Mechanics of Materials*, 7 edn, McGraw-Hill Education, New York.

Gemi, L., Madenci, E. and Özkılıç, Y. O. (2021), 'Experimental, analytical and numerical investigation of pultruded gfrp composite beams infilled with hybrid frp reinforced concrete', *Engineering Structures* **244**.
URL: *https://doi.org/10.1016/j.engstruct.2021.112790*

Gere, J. M. and Goodno, B. J. (2012), *Mechanics of Materials*, 8 edn, Cengage Learning, Stamford, CT.

Hadi, S., Kazeminezhad, E. and Safakhah, S. (2022), 'Full-scale experimental evaluation of flexural strength and ductility of reinforced concrete beams strengthened with various frp mechanisms', *Structures* **43**, 1160–1176.
URL: *https://doi.org/10.1016/j.istruc.2022.07.011*

Hijriah, Parung, H., Djamaluddin, R. and Irmawati, R. (2019), 'Delaminasi lembar gfrp pada balok beton bertulang', *Jurnal Ecosystem* **19**, 360–366.

Mirdan, D. and Saleh, A. R. (2022), 'Flexural performance of reinforced concrete (rc) beam strengthened by uhpc layer', *Case Studies in Construction Materials* **17**, e01655.
URL: *https://doi.org/10.1016/j.cscm.2022.e01655*

Mohd Hashim, M. H., Mohd Sam, A. R., Hussin, M. and Arshad, M. (2013), 'Structural performance and ductility of fiber reinforced polymer concrete bonding system under tropical climates', *Jurnal Teknologi* **61**.
URL: *https://doi.org/10.11113/jt.v61.1765*

Monier, A., Zhe, X., Huang, H. and Zhishen, W. (2017), 'External flexural strengthening of rc beams using bfrp grids and pcm', *Journal of Japan Society of Civil Engineers, Ser. A2 (Applied Mechanics)* **73**(2), I_417–I_427.
URL: *https://doi.org/10.2208/jscejam.73.i*$_4$17

Mosley, W. H., Bungey, J. H. and Hulse, R. (2012), *Reinforced Concrete Design*, CRC Press.
URL: *https://doi.org/10.1201/9781003415398*

Muflikhun, M. A. and Fiedler, B. (2022), 'Failure prediction and surface characterization of gfrp laminates: A study of stepwise loading', *Polymers* **14**(20).
URL: *https://doi.org/10.3390/polym14204322*

Nayak, A. N., Kumari, A. and Swain, R. B. (2018), 'Strengthening of rc beams using externally bonded fibre reinforced polymer composites', *Structures* **14**, 137–152.
URL: *https://doi.org/10.1016/j.istruc.2018.03.004*

Ogboin, A. S., TrustGod, J. A. and Divine, E. U. (2021), 'Shear strengthening of reinforced concrete beams with different glass fiber fabric strip width and adhesive thickness'.
URL: *https://www.jmess.org/*

Palanivel, S. and Sekar, M. (2013), 'Flexural and plastic hinge behaviour of gfrp confined frc beams', *Advanced Materials Research* **838–841**, 448–453.
URL: *https://doi.org/10.4028/www.scientific.net/AMR.838-841.448*

Paulay, T. and Priestley, M. J. N. (1992), *Seismic Design of Reinforced Concrete and Masonry Buildings*, John Wiley & Sons.

Priestley, M. J. N., Calvi, G. M. and Kowalsky, M. J. (2007), *Displacement-Based Seismic Design of Structures*, IUSS Press.

Rahman, M. J., Hasrul, M. R., Ashad, H., Yusuf, F. A. and Hasrul, N. R. (2024), 'An assessment of derelict building constructions situated in coastal regions', *Journal of the Civil Engineering Forum* **10**(3), 229–238.
URL: *https://doi.org/10.22146/jcef.10433*

Saleem, M. U., Khurram, N., Amin, M. N. and Khan, K. (2019), 'Finite element simulation of rc beams under flexure strengthened with different layouts of externally bonded fiber reinforced polymer (frp) sheets', *Revista de la Construccion* **17**(3), 383–400.
URL: *https://doi.org/10.7764/RDLC.17.2.383*

Saravanakumar, P., Chitra, N. R. and Murugesan, R. (2014), 'Comparative experimental investigation on the behaviour and strength of rc frames strengthened and retrofitted with gfrp composites', *KSCE Journal of Civil Engineering* **18**(6), 1805–1812.
URL: *https://doi.org/10.1007/s12205-014-0198-7*

Scott, B. D. (1980), Stress-Strain Relationships for Confined Concrete: Rectangular Sections, PhD thesis, The University of Canterbury.

Siswosukarto, S., Setiawan, A. F., Darmawan, M. F., Muflikhun, M. A. and Faveryan, I. B. (2024), 'Experimental and numerical simulation of gfrp confined cylindrical concrete under compression', *International Journal of GEOMATE* **27**(119), 50–58.
URL: *https://doi.org/10.21660/2024.119.4374*

Tanjung, J. and Putri, N. T. (2023), 'Identifikasi penyebab kerusakan konstruksi bangunan beton bertulang pasca bencana gempa bumi', *Jurnal Bangunan, Konstruksi & Desain* **1**(2), 72–78.
URL: *https://doi.org/10.25077/jbkd.1.2.72-78.2023*

Zhu, H., Li, Z., Chen, Q., Cheng, S., Li, C. and Zhou, X. (2022), 'A new analytical model for deflection of concrete beams reinforced by bfrp bars and steel fibres under cyclic loading', *Polymers* **14**(9).
URL: *https://doi.org/10.3390/polym14091797*